

## Electronic Supporting Information (ESI) Rigidity and fracture of fibrous double networks

Pancy Lwin,<sup>1</sup> Andrew Sindermann,<sup>1</sup> Leo Sutter,<sup>1</sup> Thomas Wyse  
Jackson,<sup>2</sup> Lawrence Bonassar,<sup>3</sup> Itai Cohen,<sup>2</sup> and Moumita Das<sup>1</sup>

<sup>1</sup>*School of Physics and Astronomy, Rochester Institute of Technology, Rochester, NY 14623, USA*

<sup>2</sup>*Department of Physics, Cornell University, Ithaca, NY 14853, USA*

<sup>3</sup>*Meinig School of Biomedical Engineering and Sibley School of Mechanical  
and Aerospace Engineering, Cornell University, NY 14853, USA*

(Dated: November 25, 2021)

### CONTENTS

1. SI Movie 1: Deformation and fracture of the DN in response to uniaxial strain applied at the boundary and increased in steps of 1%. The bond occupation probability of the stiff (black) network was set to  $p_1 = 0.62$  and the bond occupation probability of the flexible (blue) network was set to  $p_2 = 0.60$ .
2. This Supplementary Information Document.

### IMPACT OF VARYING THE INTER-NETWORK INTERACTION ON THE MECHANICS OF THE MODEL DN

In the main manuscript, we set the elastic interaction between the two networks  $\alpha_3/\alpha_1 = 1.1$ , with the assumption that one could think of  $\alpha_3$  as an effective spring for the springs  $\alpha_1$  and  $\alpha_2$  acting in parallel. Here we relax this assumption, and discuss results for  $\alpha_3/\alpha_1 \sim 0.001 - 1$ . We find that varying  $\alpha_3/\alpha_1$  does not affect the main conclusion of our paper namely that: the secondary flexible network modulates the mechanics of the composite DN far more effectively when the primary stiff network is near its rigidity threshold. However,  $\alpha_3/\alpha_1$  can be used to tune the micromechanics of the network.

In figures 1 and 2 we present data for  $\alpha_3/\alpha_1 = 0.01$ . These figures show that normalized Young's modulus and strain at maximum stress show significant variation with  $p_2$ , when  $p_1$  is 0.62 but not when it is 0.80, as in the main manuscript. In addition, the rigidity percolation threshold on the DN remains the same. In figure 3, we present the variation of the normalized shear modulus with  $p_1$  for different values of  $p_2$  for two cases; when  $\alpha_3/\alpha_1 = 0.01$  and when it is 0.001. The rigidity percolation thresholds for a given  $p_2$  does not depend on  $\alpha_3/\alpha_1$ . This is expected because the percolation threshold is set by the balance between the degrees of freedom and constraints in the system. Finally, varying the coupling between the networks does impact the values of the Young's modulus, the maximum stress, and the strain at maximum stress as seen in Fig. 4. A weaker coupling (smaller  $\alpha_3$ ) allows for more non-affine deformations of the DN and thus leads to a decrease in its Young's modulus (rigidity), maximum stress (strength) and an increase in the strain at maximum stress (extensibility).

These results show that in addition to the axial rigidities of the filaments in the two networks  $\alpha_1$  and  $\alpha_2$ , the coupling strength  $\alpha_3$  can modulate deformations and relaxation of the network. Note, however, that the bonds corresponding to  $\alpha_3$  are present only if the corresponding bonds in the two networks, are both present, i.e., there is no independent source of disorder in the coupling between the networks. Therefore, changing  $\alpha_3$  can only change the shape of the modulus versus bond occupation probability curves and not the rigidity percolation threshold of the composite network for small deformations of the DN when there is no breaking or buckling of bonds.

### IMPACT OF VARYING THE RATIO OF FILAMENT STRETCHING STIFFNESSES OF THE TWO NETWORKS

For large deformations that result in breaking and buckling of bonds, we found that changing  $\alpha_2/\alpha_1$  will change the shape of the modulus versus strain, and stress versus strain curves, and consequently the values of maximum or peak stress, and the strain at maximum stress, but the qualitative trends remain unchanged. To illustrate this, in Fig.5, we show results from simulations where we set the above-mentioned ratio to 0.2 instead of 0.1 as in the manuscript. Further, we ran these simulations for  $p_1 = 0.7$  in addition to for  $p_1 = 0.62$  and  $p_1 = 0.8$ . In Fig.5, panels (a), (b),

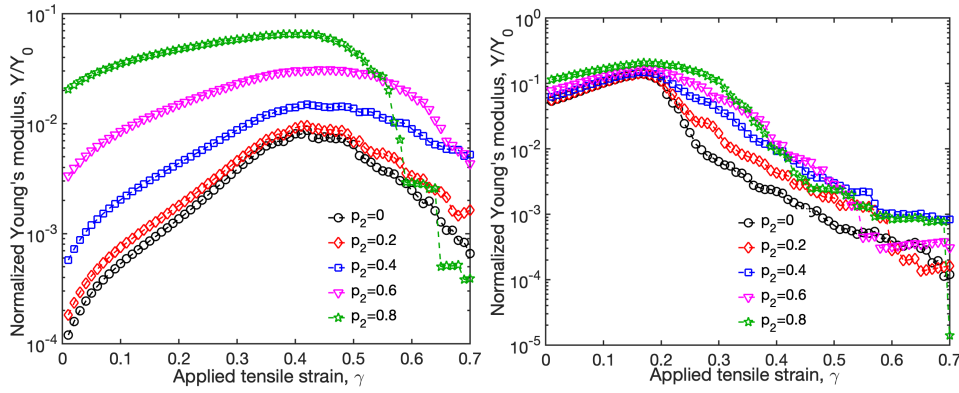


FIG. 1. The normalized Young's modulus ( $Y/Y_0$ ) shown as a function of the applied tensile strain,  $\gamma$ , for the bond occupation probability of the stiff network  $p_1 = 0.62$  (left figure) and  $p_1 = 0.8$  (right figure). The flexible network has a bond occupation probability,  $p_2$  as shown in the legend. The parameters are:  $\alpha_2/\alpha_1 = 0.1$ ,  $\kappa/\alpha_1 = 0.004$ , and  $\alpha_3/\alpha_1 = 0.01$ .

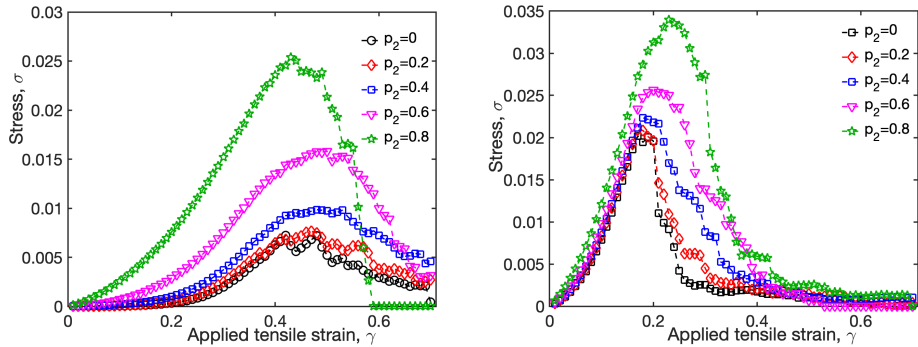


FIG. 2. The stress  $\sigma$  shown as a function of the applied tensile strain,  $\gamma$ , for the bond occupation probability of the stiff network  $p_1 = 0.62$  (left figure) and  $p_1 = 0.8$  (right figure). The flexible network has a bond occupation probability,  $p_2$  as shown in the legend. The parameters are:  $\alpha_2/\alpha_1 = 0.1$ ,  $\kappa/\alpha_1 = 0.004$ , and  $\alpha_3/\alpha_1 = 0.01$ .

and (c) show the modulus as a function of applied strain, and panels (d), (e), and (f) show the stress as a function of applied strain, where the open symbols correspond to a ratio  $\alpha_2/\alpha_1$  of 0.1 and the closed symbols to 0.2. Note that while changing the value of  $\alpha_2/\alpha_1$  led to small quantitative changes (larger rigidities and load bearing capability for  $\alpha_2/\alpha_1 = 0.2$ ), it did not change the qualitative trends reported in the manuscript. To further crosscheck this, we also examine the peak or maximum stress the DN can withstand before it starts to soften, and the strain at maximum stress. We show these results in Fig.6. As expected, we found that the peak stresses are larger when  $\alpha_2/\alpha_1 = 0.2$  than when  $\alpha_2/\alpha_1 = 0.1$ , but the qualitative trends remain the same. Similarly, the qualitative trends for the strain at maximum stress also remain the same, although there are small quantitative changes.

## IMPACT OF VARYING THE BOND OCCUPATION PROBABILITY OF THE STIFF NETWORK

We first show data for values of  $p_1$  close to the rigidity percolation threshold of the primary network ( $p_c \sim 0.58$  in our simulations) with  $p_2$  set to 0. In Fig.7 below, we show the data, averaged over five runs, for the normalized shear modulus,  $G/G_0$  as a function of  $|p_1 - p_c|$  for the two extreme cases:  $p_2 = 0$  and  $p_2 = 1$ . Note that while for both  $p_2 = 0$  in Fig.7 (a) and  $p_2 = 1$  Fig.7 (b),  $G/G_0$  first increases very slowly (when  $|p_1 - p_c|$  is 0.001 or less), then more rapidly, the increase spans many more decades for  $p_2 = 0$ . This is also clearly seen in difference in the logarithms of the normalized shear modulus for  $p_2 = 1$  and  $p_2 = 0$ , shown in Fig.7 (c), as a function of  $|p_1 - p_c|$ . As expected very close to a phase transition, this difference is large when  $|p_1 - p_c| = 10^{-4}$  (and  $\sim$  over 5 orders of magnitude difference in the normalized shear modulus), and then decreases steadily as we move away from  $p_c$ ; when we reach  $|p_1 - p_c| = 10^{-1}$ , the two normalized moduli differ only by an order of magnitude. These trends are corroborated data for the corresponding data for the peak stress for large deformations leading to fracture shown in Fig.8.

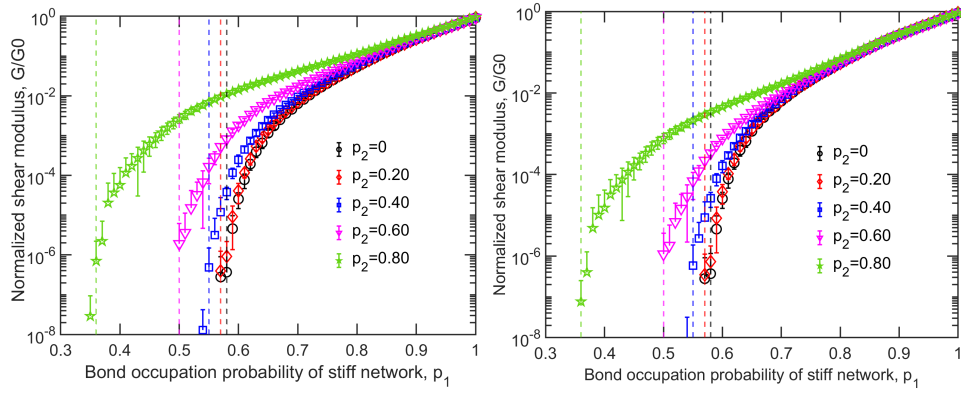


FIG. 3. The normalized shear modulus ( $G/G_0$ ) shown as a function of the occupation probability,  $p_1$ , of the stiff network for two different  $\alpha_3/\alpha_1$ , 0.01 (left figure) and 0.001 (right figure). The flexible network has a bond occupation probability,  $p_2$  as shown in the legend. The parameters are:  $\alpha_2/\alpha_1 = 0.1$  and  $\kappa/\alpha_1 = 0.004$ . The applied shear strain is 0.05.

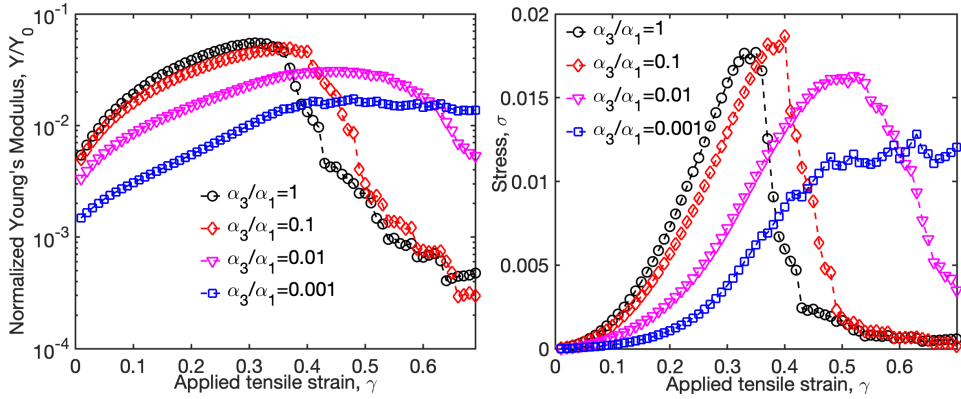


FIG. 4. The normalized Young's modulus,  $Y/Y_0$ , and stress,  $\sigma$ , as functions of the uniaxial tensile strain  $\gamma$  applied at the boundaries. In this figure,  $p_1 = 0.62$  and  $p_2 = 0.60$ , and  $\alpha_3/\alpha_1$  has values as shown in the legend.

Next, we show data for four different values of  $p_1$ , 0.62, 0.63, 0.7, 0.8, from near  $p_c$  to far away from  $p_c$ . We show the variation in  $dG/dp_2$  as a function of  $p_2$  in Fig.9, the normalized Young's modulus vs. strain in Fig.10 (a-d), stress vs strain in Fig.11(a-d), peak stress vs  $p_2$  in Fig.12 (a), and strain at maximum stress vs  $p_2$  in Fig.12 (b). In all these figures. we observe large variations in the DN's properties for  $p_1 = 0.62$  and 0.63, and and these variations are attenuated as  $p_1$  is increased, with rather small variations for  $p_1 = 0.8$ . These results corroborate the main finding of the paper that the tunability of network mechanics and fracture properties is most striking when the primary network is near its rigidity percolation threshold.

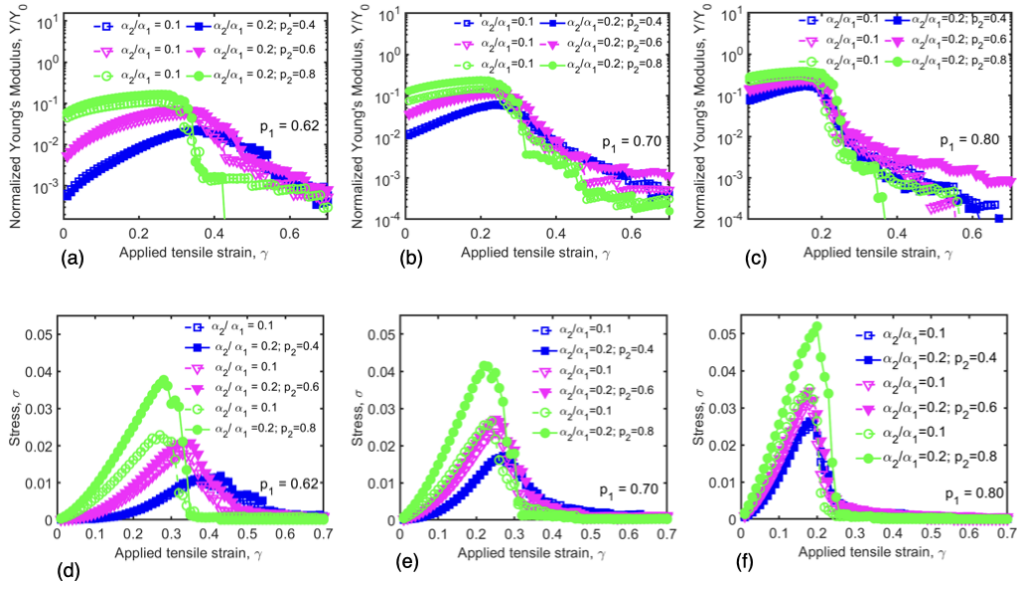


FIG. 5. The normalized Young's modulus,  $Y/Y_0$ , and stress,  $\sigma$ , as functions of the uniaxial tensile strain  $\gamma$  applied at the boundaries, for three different values of  $p_1$ . The ratio  $\alpha_2/\alpha_1$  has values as shown in the legend.

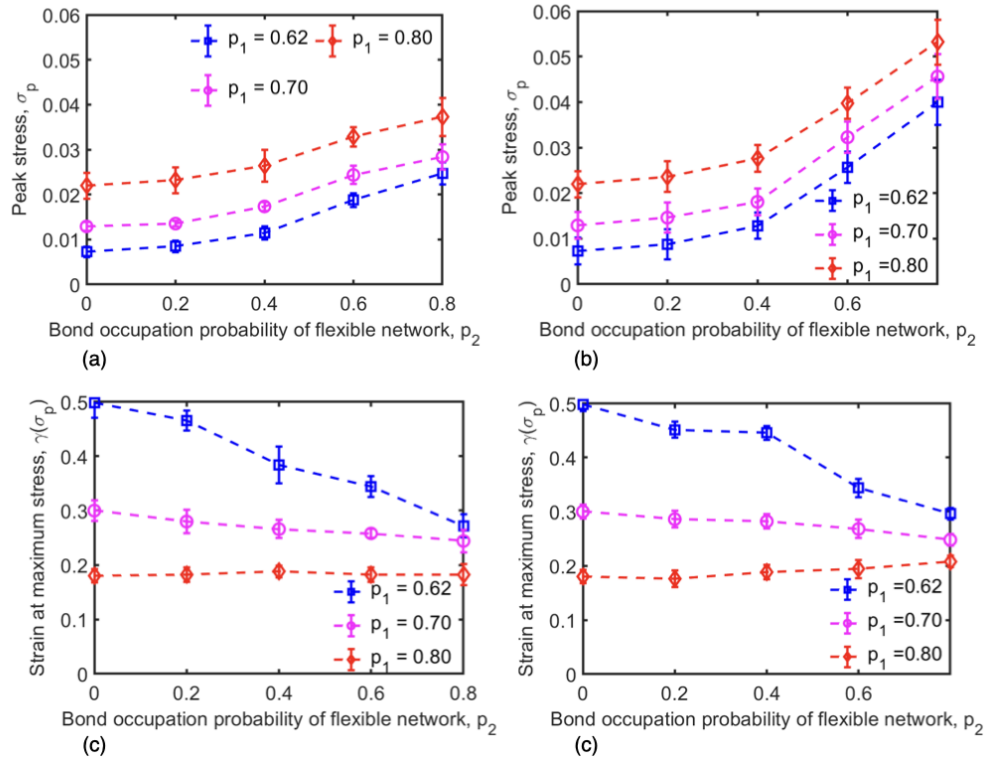


FIG. 6. The peak stress and strain at maximum stress as functions of bond occupation probability of the flexible network  $p_2$ . Panels (a) and (b) show the peak stress when  $\alpha_2/\alpha_1 = 0.1$  and  $0.2$ , respectively, while Figures (c) and (d) show the respective strain at maximum stress. The data presented represent three values of  $p_1$  shown in the legend.

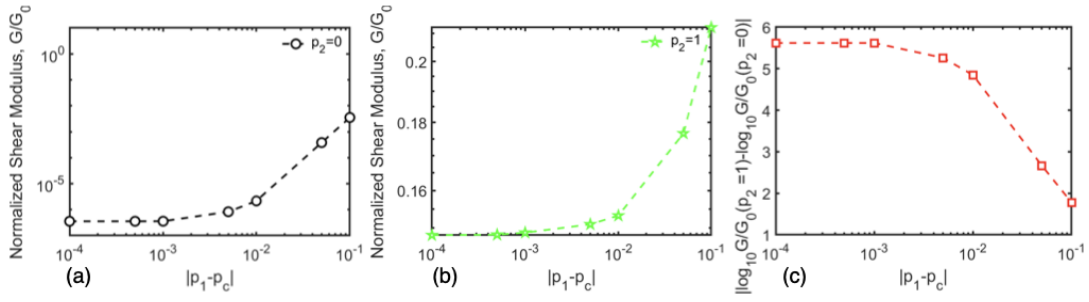


FIG. 7. Figure shows the normalized shear modulus ( $G/G_0$ ) as a function of the deviation from the bond occupation probability  $p_1$  from the rigidity percolation threshold  $p_c$  ( $\sim 0.58$ ) for  $p_2 = 0$ , for the two extreme cases of  $p_2 = 0$  in (a) and  $p_2 = 1$  in (b). In figure (c), we show the difference in the logarithm of the normalized modulus values for the occupation probabilities shown in (a) and (b).

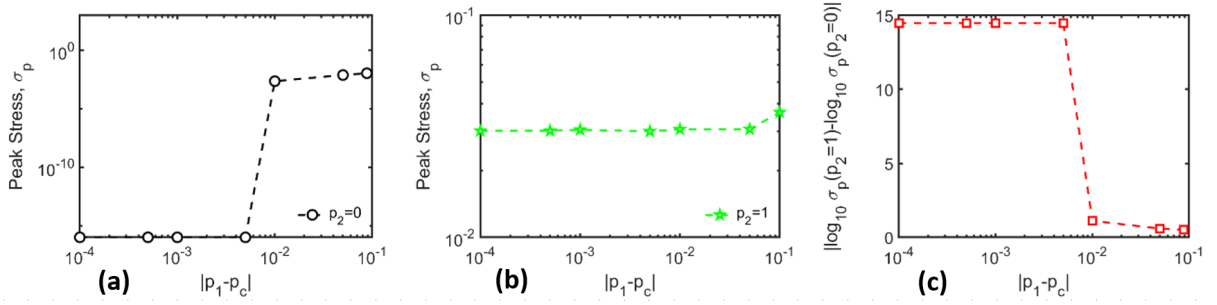


FIG. 8. Figure shows the peak stress as a function of  $|p_1 - p_c|$ , where ( $p_c \sim 0.58$ ) for the two extreme cases of  $p_2 = 0$  in (a) and  $p_2 = 1$  in (b). In figure (c), we show the difference in the logarithm of the peak stress values for the occupation probabilities shown in (a) and (b).

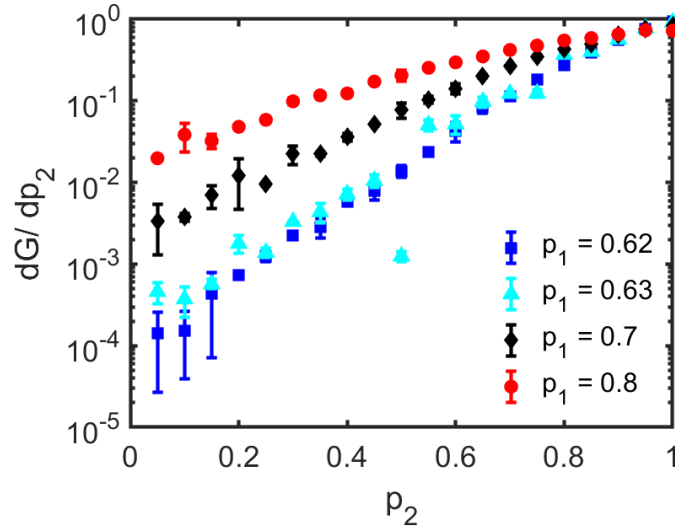


FIG. 9. Figure shows the derivative of normalized shear modulus  $G/G_0$  as a function of the bond occupation probability  $p_2$ , for different values of  $p_1$  (shown in legend).

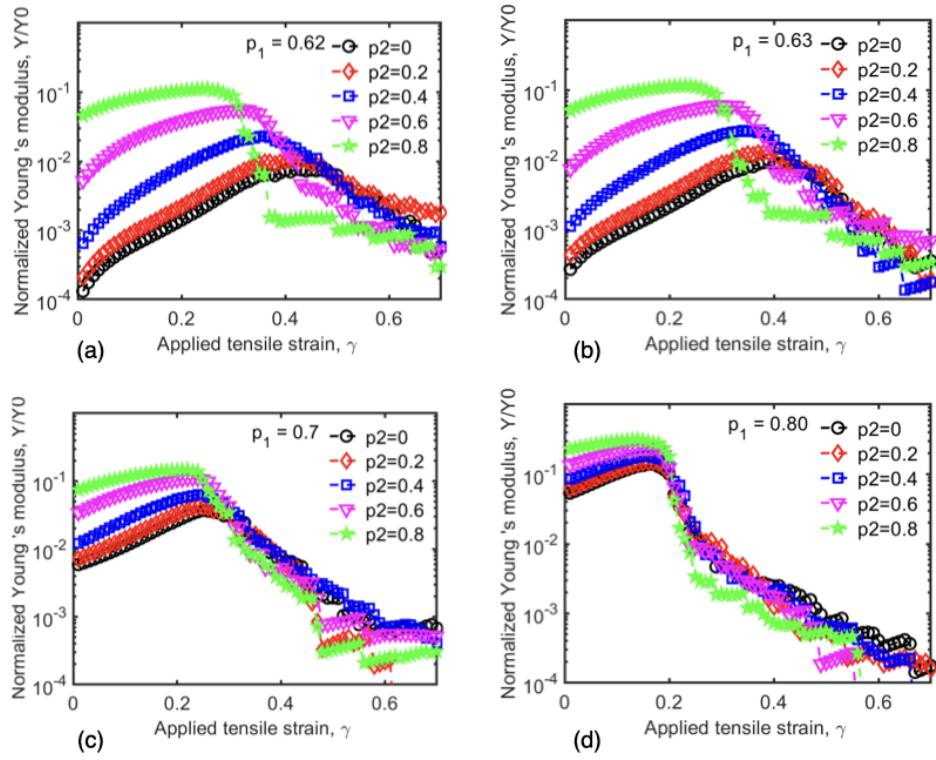


FIG. 10. Panels (a - d) shows the normalized Young's modulus  $Y/Y_0$  of the SN (black circles) and DN (remaining data) as a function of the uniaxial tensile strain  $\gamma$  which is applied at the top boundaries, with  $p_1$  set to 0.62 (a), 0.63 (b), 0.7 (c), and 0.8 (d).

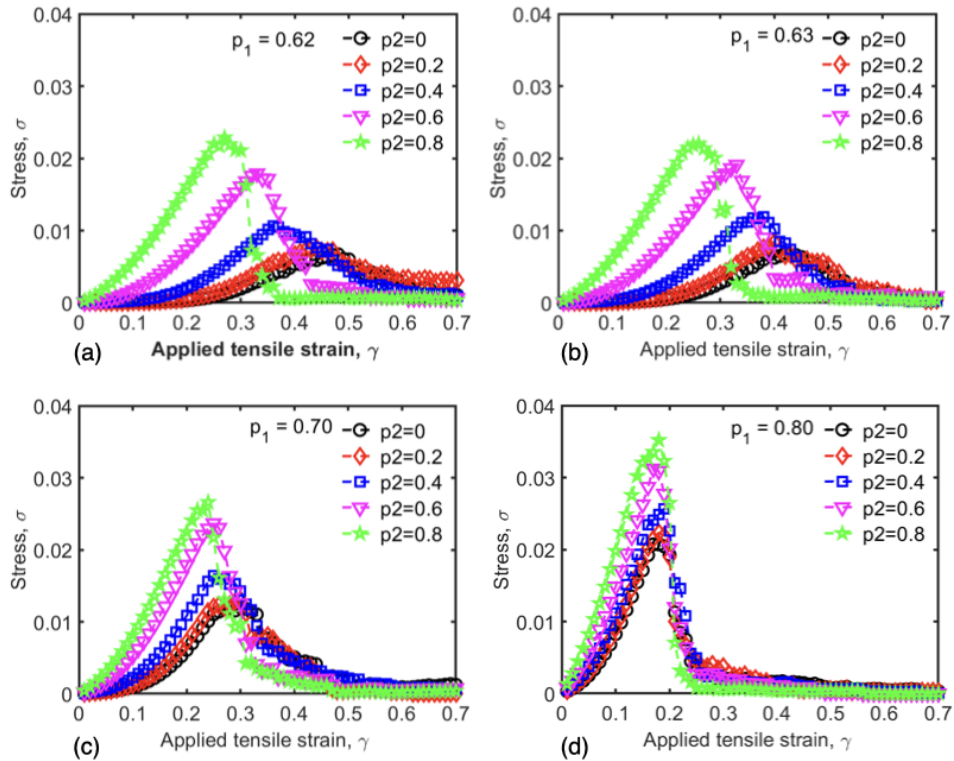


FIG. 11. Panels (a-d) shows the stress  $\sigma$  developed in the SN (black circles) and DN (remaining data) as a function of the uniaxial tensile strain  $\gamma$  which is applied at the top boundaries, with  $p_1$  set to 0.62 (a), 0.63 (b), 0.7 (c), and 0.8 (d).

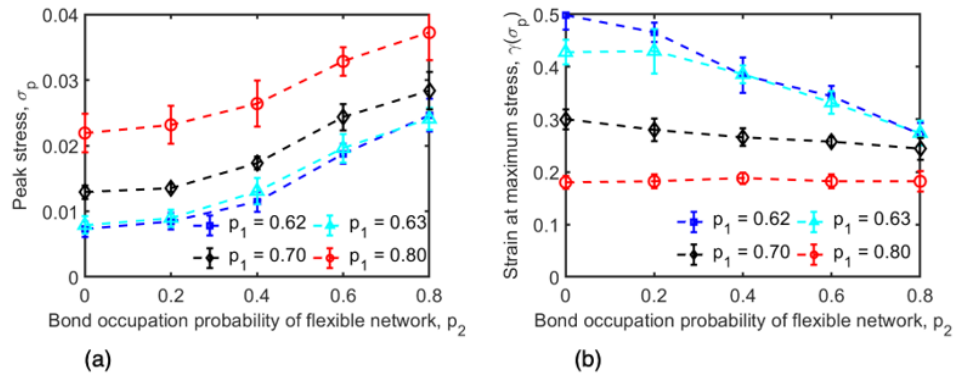


FIG. 12. Panels (a) and (b) respectively show the maximum or peak stress  $\sigma_p$  and strain at this maximum stress plotted against the bond occupation probability of flexible network  $p_2$ .